Eur. Phys. J. C (2022) 82:462
https://doi.org/10.1140/epjc/s10052-022-10420-y

THE EUROPEAN PHYSICAL JOURNAL C

Check for updates

Regular Article - Experimental Physics

Study of the KNO scaling in pp collisions at $\sqrt{s}$ from 0.9 to 13 TeV using results of the ATLAS at the LHC

Yuri Kulchitsky[a], **Pavel Tsiareshka**

Joint Institute for Nuclear Research, Dubna, Russia

Received: 28 February 2022 / Accepted: 9 May 2022 / Published online: 20 May 2022
© The Author(s) 2022

Abstract The comparisons of the charged-particle multiplicity and the average transverse momentum distributions on the scaled multiplicity, KNO scale, using the results of the ATLAS collaboration at the LHC are presented. These distributions were measured in proton–proton collisions at centre-of-mass energies from 0.9 to 13 TeV for the absolute pseudorapidity region less than 2.5 and two samples of events with each charged-particle transverse momentum greater than 100 and 500 MeV, respectively. The shape evolution of the multiplicity distributions with a collision energy is studied in terms of KNO scaling variables. The charged-particle multiplicity distributions on the KNO scale have the similar shape and decrease with increasing collision energy. The KNO distributions tend to be independent of energy for the highest energies. The average transverse momentum distributions on the KNO scale have a similar shape and increase with increasing collision energy.

1 Introduction

The study of charged-particle distributions in proton–proton (pp) collisions probes the strong interaction in the low-momentum transfer, non-perturbative region of quantum chromodynamics.

Charged-particle distributions were measured at CERN's Large Hadron Collider (LHC) [1] experiments for various centre-of-mass energies, $\sqrt{s}$, from 0.9 to 13 TeV by the ATLAS [2] Collaboration [3–7], the CMS [8] Collaboration [9–13], the CMS and TOTEM [14] Collaborations [15], the TOTEM Collaboration [16], the ALICE [17] Collaboration [18–23] and the LHCb [24] Collaboration [25,26]. Charged-particle distributions were studied by the CDF Collaboration at Tevatron (Fermilab) at $\sqrt{s} = 0.63$, 1.8 and 1.96 TeV [27,28] and by the UA1, UA4 and UA5 Collaborations at the SPS (CERN) at $\sqrt{s} = 0.2$, 0.54 and 0.9 TeV [29–32].

Measurements of charged-particle distributions in the ATLAS experiment [3–7] at centre-of-mass energies $\sqrt{s} =$ 0.9, 2.36, 7, 8 and 13 TeV were performed for the pseudorapidity region $|\eta| < 2.5$ and for two samples of events: with primary charged-particle multiplicity, $n_{\rm ch}$, more than or equal to 2 and 1 and with the each charged-particle transverse momentum $p_{\rm T}$ more than 100 and 500 MeV, respectively.

The hypothesis that at very high energies the probability distributions $P(n, \sqrt{s})$ of producing n particles in a certain collision process should exhibit a scaling relation was proposed in Refs. [33–35]. This scaling behaviour is a property of particle multiplicity distributions known as the KNO scaling hypothesis. The main assumption of KNO scaling is Feynman scaling [36], where it was concluded that for asymptotically large energies with $\sqrt{s} \to \infty$ the mean total number of any kind of particle rises logarithmically with a centre-of-mass energy as $\langle n \rangle \propto \ln \sqrt{s}$. For this assumption the multiplicity distribution $P(n, \sqrt{s})$ was represented as

$$P(n, \sqrt{s}) = \frac{1}{\langle n(\sqrt{s}) \rangle} \Psi(z) + \mathcal{O}\left(\frac{1}{\langle n(\sqrt{s}) \rangle^2}\right), \quad (1)$$

where $\langle n(\sqrt{s}) \rangle$ is the average multiplicity of primary particles at centre-of-mass energy, $\Psi(z)$ is a particle distribution as a function of the scaled multiplicity $z = n(\sqrt{s})/\langle n(\sqrt{s}) \rangle$. The first term in Eq. (1) was results from the leading term in $\ln \sqrt{s}$ (KNO scaling hypothesis) and the second term contains all other terms [37]. The multiplicity distributions become simple rescaled copies of the universal function $\Psi(z)$ depending only on the scaled multiplicity or an energy-independent function. Asymptotically for $\sqrt{s} \to \infty$ the second term in Eq. (1) tends to zero and therefore KNO scaling holds.

The energy independence of the moments $C_{\rm q}(\sqrt{s}) = \langle n^q(\sqrt{s}) \rangle / \langle n(\sqrt{s}) \rangle^q$ in an energy asymptotic, $\sqrt{s} \to \infty$, was the precise finding of the KNO scaling [34]. The introduction of the novel physically well-motivated scaling rules for high-energy data was presented in Ref. [38].

[a] e-mail: Iouri.Koultchitski@cern.ch (corresponding author)

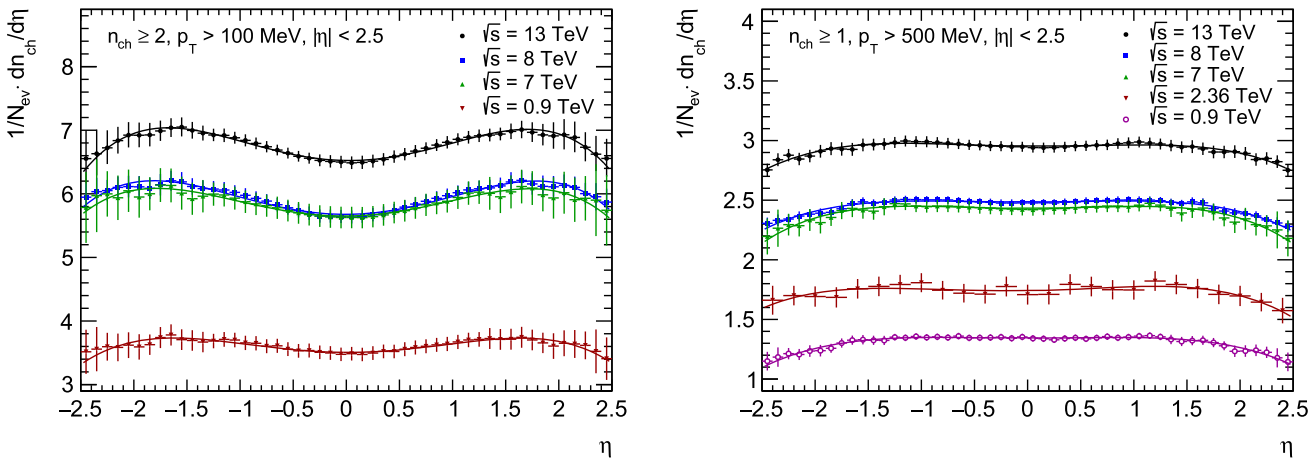

Fig. 1 The primary charged-particle average multiplicity, $1/N_{ev} \cdot dn_{ch}/d\eta$, dependence on pseudorapidity region $-2.5 < \eta < 2.5$ for the ATLAS Collaboration results for the charged-particle with **a** $n_{ch} \geq 2$, $p_T > 100$ MeV and **b** $n_{ch} \geq 1$, $p_T > 500$ MeV at centre-of-mass energies $\sqrt{s} = 0.9, 2.36, 7, 8$ and 13 TeV [3–7]. The coloured symbols represent the data. The vertical bars represent statistical and systematic uncertainties added in quadrature. The black curves show the results of the fits with the fourth-degree polynomial function

The KNO scaling was studied at the LHC energies by the CMS [11] and the ALICE [18,21] Collaborations. The KNO scaling violation were observed for a larger rapidity range in LHC experiments at centre-of-mass energies $\sqrt{s} = 0.9$–8 TeV [11,18,21].

Charged-particle multiplicity and transverse momentum distributions in pp collisions at centre-of-mass energies $\sqrt{s} = 0.2$–14 TeV within the Monte Carlo Quark-Gluon String Model (MC QGSM) [39,40] based on Gribov's Reggeon field theory [41,42] were studied in Refs. [43,44], where special attention was given to the origin of violation of the KNO scaling. Detailed theoretical description of the KNO scaling was done in Refs. [37,45,46].

This publication presents in Sect. 2 the comparison of the charged-particle distributions as a function on the KNO scale, in Sect. 3 the study of the KNO scaling and in Sect. 4 the comparison of the average transverse momentum of the primary charged particles as a function on the KNO scale based on the results of the ATLAS Collaboration. The moments C_q were not studied by the ATLAS Collaboration and is not discussed in the paper.

2 Charged-particle multiplicity distributions

The measurements used for the analysis are the data on pp collisions at $\sqrt{s} = 0.9$–13 TeV recorded by the ATLAS experiment [2] at the LHC [1] in 2010–2015 [3–7]. The data were taken in the special configuration of the LHC with low beam currents and reduced beam focusing, producing a low mean number of interactions per bunch-crossing in the range 0.003–0.007.

The following measured observables are used in the analysis: $P(n_{ch}, \sqrt{s}) = (dN_{ev}(\sqrt{s})/dn_{ch})/N_{ev}(\sqrt{s})$ and $\langle p_T(n_{ch}, \sqrt{s})\rangle$, where N_{ev} is the number of events with primary charged particles in the kinematic acceptance, n_{ch} is the number of primary charged particles within the kinematic acceptance in an event and $\langle p_T(n_{ch}, \sqrt{s})\rangle$ is the average momentum component transverse to the beam direction for charged particles in an event at centre-of-mass energy $\sqrt{s}$.

As was defined in Sect. 1, for the verification of the KNO scaling hypothesis the following equation with dependence from a centre-of-mass energy, $\sqrt{s}$, and a kinematic region, p_T^{min}, was used:

$$\Psi(z, \sqrt{s}) = \langle n_{ch}(\sqrt{s}, p_T^{min})\rangle P(n_{ch}, \sqrt{s}, p_T^{min}) = \frac{\langle n_{ch}(\sqrt{s}, p_T^{min})\rangle}{N_{ev}(\sqrt{s}, p_T^{min})} \cdot \frac{dN_{ev}(\sqrt{s}, p_T^{min})}{dn_{ch}}. \quad (2)$$

For correct comparison of charged-particle multiplicity and average transverse momentum distributions for different energies or kinematic regions the scaled multiplicity is introduced as follows:

$$z = \frac{n_{ch}(\sqrt{s}, p_T^{min})}{\langle n_{ch}(\sqrt{s}, p_T^{min})\rangle}. \quad (3)$$

For example, comparison of results for different kinematic regions, with two p_T^{min} thresholds, was presented in Ref. [47].

A fit with a fourth-degree polynomial function of the primary charged-particle average multiplicity distributions in the pseudorapidity region $-2.5 < \eta < 2.5$ was used for the

Table 1 The average multiplicity, $\langle n_{\rm ch}(\sqrt{s}, p_{\rm T}^{\rm min})\rangle$, as the results of the fits with a polynomial function of the primary charged-particle average multiplicity distributions on pseudorapidity region $-2.5 < \eta < 2.5$ for the events samples with $p_{\rm T} > 100$ MeV and $p_{\rm T} > 500$ MeV at centre-of-mass energies $\sqrt{s} = 0.9$, 2.36, 7, 8 and 13 TeV using the ATLAS Collaboration results [3–7]

$\sqrt{s}$ [TeV]	$p_{\rm T}^{\rm min}$ [MeV]	Average multiplicity $\langle n_{\rm ch}(\sqrt{s}, p_{\rm T}^{\rm min})\rangle$	Relative uncertainty $\frac{\delta\langle n_{\rm ch}(\sqrt{s}, p_{\rm T}^{\rm min})\rangle}{\langle n_{\rm ch}(\sqrt{s}, p_{\rm T}^{\rm min})\rangle}$
13	100	33.88 ± 0.11	0.0032
	500	14.66 ± 0.04	0.0027
8	100	29.81 ± 0.10	0.0034
	500	12.25 ± 0.03	0.0024
7	100	29.40 ± 0.19	0.0065
	500	11.98 ± 0.05	0.0042
2.36	500	8.66 ± 0.51	0.0589
0.9	100	18.06 ± 0.12	0.0066
	500	6.53 ± 0.03	0.0046

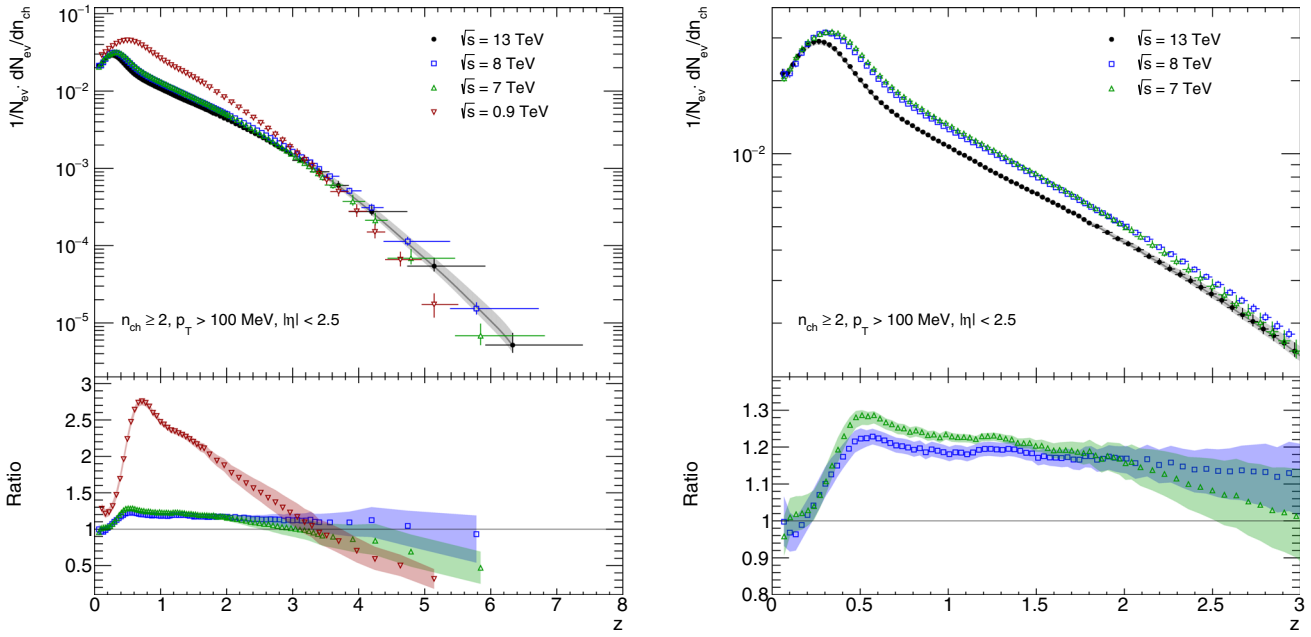

Fig. 2 Top panel: Primary charged-particle multiplicity distributions as a function of the scaled multiplicity z, defined in Eq. (3), for events with $n_{\rm ch} \geq 2$, $p_{\rm T} > 100$ MeV and $|\eta| < 2.5$ measurement at the centre-of-mass energies 0.9, 7, 8 and 13 TeV by the ATLAS [3–7] in **a** complete multiplicity region and **b** zoom multiplicity region with $z \leq 3$ at the $\sqrt{s} = 7$, 8 and 13 TeV. The gray curve and band of the uncertainties are the result of the interpolation of the charged-particle multiplicity distribution at 13 TeV. The error bars and boxes represent the statistical and systematic contributions, respectively. Bottom panel: The ratios of the charged-particle multiplicity distributions to the interpolated distribution at $\sqrt{s} = 13$ TeV are shown. Bands represent the uncertainties for the ratios as results of statistical and systematic uncertainties added in quadrature for both distributions

calculation of an average multiplicity, $\langle n_{\rm ch}(\sqrt{s}, p_{\rm T}^{\rm min})\rangle$, for different centre-of-mass energies and $p_{\rm T}^{\rm min}$ using the ATLAS results [3–7]. The $1/N_{\rm ev} \cdot dn_{\rm cn}/d\eta$ distributions on pseudorapidity are shown in Fig. 1. The average multiplicity, $\langle n_{\rm ch}(\sqrt{s}, p_{\rm T}^{\rm min})\rangle$, as the results of these distributions fit with fourth-degree polynomial function are presented in Table 1. The χ^2/ndf is good for all fits. The average multiplicity as the results of the sum of these distributions agree with the fit results up to the third digit after coma. Therefore the systematic uncertainties for average multiplicities calculated using these methods is negligible.

The comparison of the primary charged-particle multiplicities as a function of the scaled multiplicity z or KNO scale, defined in Eq. (3), for events with $n_{\rm ch} \geq 2$ and $p_{\rm T} > 100$ MeV; $n_{\rm ch} \geq 1$ and $p_{\rm T} > 500$ MeV for $|\eta| < 2.5$ measurement by ATLAS Collaboration at the $\sqrt{s}$ from 0.9 to 13 TeV [3–7] are presented in Figs. 2 and 3, respectively. For these figures the multiplicity axis was compressed by the factor $\langle n_{\rm ch}(\sqrt{s}, p_{\rm T}^{\rm min})\rangle$. KNO scale is the same and therefore

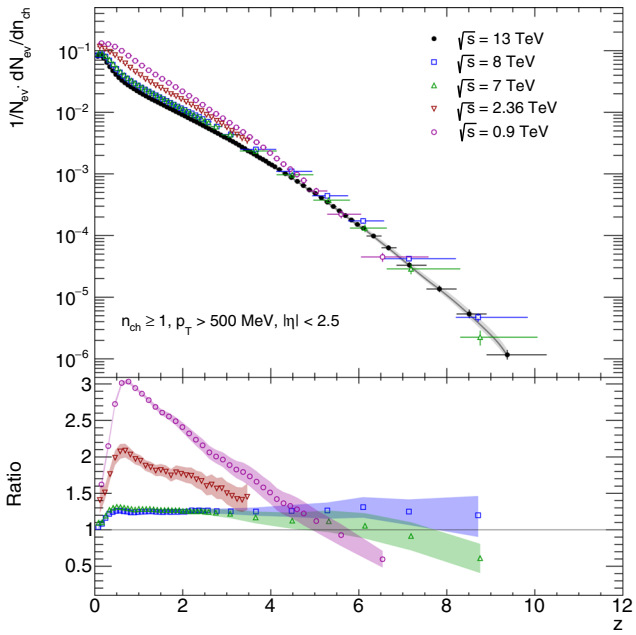

(a)

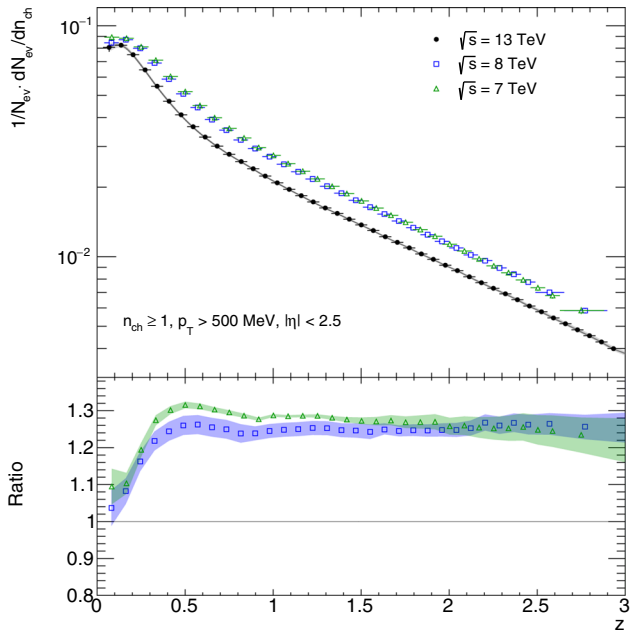

(b)

Fig. 3 Top panel: Primary charged-particle multiplicity distributions as a function of the scaled multiplicity z, defined in Eq. (3), for events with $n_{\rm ch} \geq 1$, $p_{\rm T} > 500$ MeV and $|\eta| < 2.5$ measurement at the centre-of-mass energies 0.9, 2.36, 7, 8 and 13 TeV by the ATLAS [3–7] in **a** complete multiplicity region and **b** zoom multiplicity region with $z \leq 3$ at the $\sqrt{s} = 7$, 8 and 13 TeV. The gray curve and band of the uncertainties are the result of the interpolation of the charged-particle multiplicity distribution at 13 TeV. The error bars and boxes represent the statistical and systematic contributions, respectively. Bottom panel: The ratios of the charged-particle multiplicity distributions to the interpolated distribution at $\sqrt{s} = 13$ TeV are shown. Bands represent the uncertainties for the ratios as results of statistical and systematic uncertainties added in quadrature for both distributions

it is the correct scale for comparing distributions at different center-of-mass energies or distributions in different kinematic regions.

The scaled multiplicity regions are up to 7.5 average multiplicity for $p_{\rm T} > 100$ MeV and up to 10.5 average multiplicity for $p_{\rm T} > 500$ MeV as shown in Figs. 2a and 3a, respectively.

In Table 1 the relative uncertainty, $\delta\langle n_{\rm ch}\rangle/\langle n_{\rm ch}\rangle$, is for average multiplicities. Relative uncertainties are small and equal to 0.32–0.66% for $p_{\rm T} > 100$ MeV and 0.24–0.46% for $p_{\rm T} > 500$ MeV, except result at $\sqrt{s} = 2.36$ GeV which was measured with the worst accuracy. The relative uncertainty for a bin size, $\delta z/\Delta z$, of KNO variable z is equal to $\delta\langle n_{\rm ch}\rangle/\langle n_{\rm ch}\rangle$. Therefore influence of average multiplicity uncertainties presented in Table 1 on KNO scale are very small.

In the bottom panels ratios of charged-particle distributions at 0.9–8 TeV to the distribution at 13 TeV are shown. Ratios, and their uncertainties, of charged-particle distributions at smaller centre-of-mass energies to the distribution at 13 TeV, which was obtained by interpolation, are presented in Figs. 2, 3 and following figures in Sects. 3 and 4. For the interpolation procedure the INTERPOLATOR method of the ROOT statistical analysis framework [48] was used. Figures 2, 3, 4, 5 and 6 show the gray curve and band of the uncertainties as the result of the interpolation of the distribution at 13 TeV.

Figures 2 and 3 show that primary charged-particle multiplicity distributions decrease as collision energy increases from 0.9 to 13 TeV on the factor of ≈ 3 for maximum at $z \approx 0.7$.

The results for the $\sqrt{s} = 7$, 8 and 13 TeV and $z \leq 3$ are presented in Fig. 2b for $p_{\rm T} > 100$ MeV and Fig. 3b for $p_{\rm T} > 500$ MeV. One can see that for the distributions at $\sqrt{s} = 7$ and 8 TeV there is agreement within error bars except for region $0.5 < z < 1.5$. The multiplicity distribution at 8 TeV is $\approx 20\%$ larger than at 13 TeV for region the $z < 3$ in both cases.

3 Study of the KNO scaling

The KNO scale variable z in Eq. (3) provides the way to study the evolution of the shape of KNO charged-particle multiplicity distributions (2) with varying centre-of-mass energy and kinematic region, for example $p_{\rm T}$ threshold. The KNO distributions (2) and their ratios are presented in Fig. 4 for charged particles with $p_{\rm T} > 100$ MeV and Fig. 5 for charged

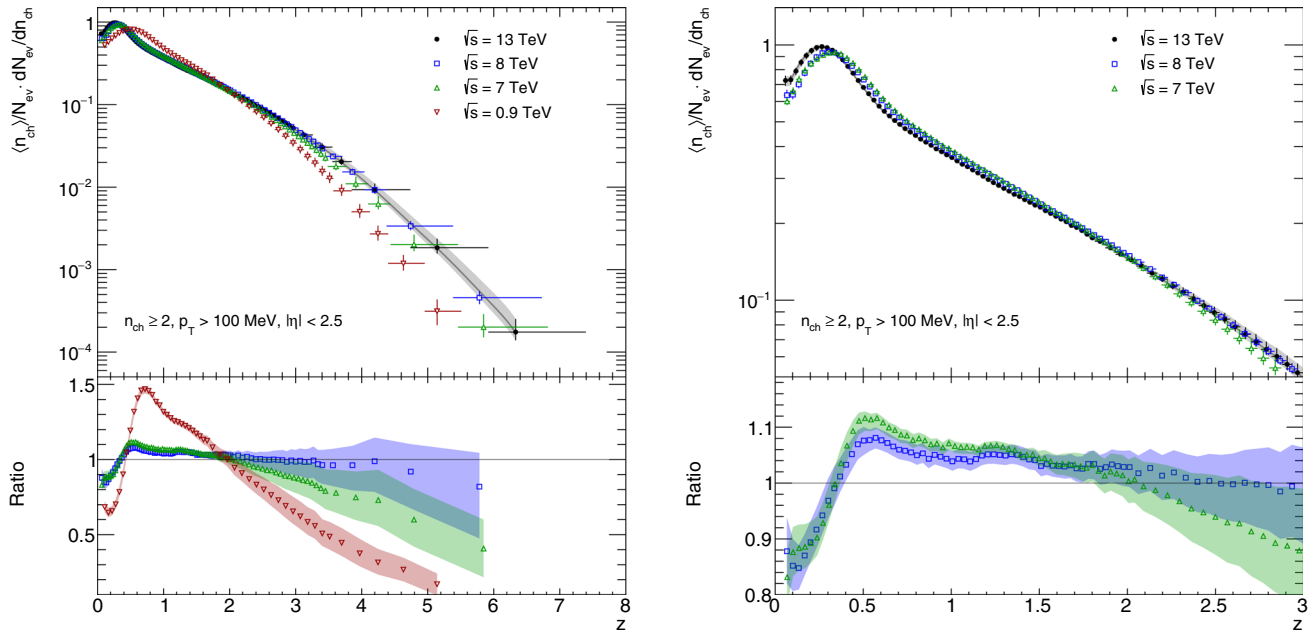

Fig. 4 Top panel: KNO scaled primary charged-particle multiplicity distributions as a function of the scaled multiplicity z, defined in Eq. (3), for events with $n_{\mathrm{ch}} \geq 2$, $p_{\mathrm{T}} > 100$ MeV and $|\eta| < 2.5$ measurement at the centre-of-mass energies 0.9, 7, 8 and 13 TeV by the ATLAS [3–7] in **a** complete multiplicity region and **b** zoom multiplicity region with $z \leq 3$ at the $\sqrt{s} = 7$, 8 and 13 TeV. The gray curve and band of the uncertainties are the result of the interpolation of the charged-particle multiplicity distribution at 13 TeV. The uncertainties represent the sum in quadrature of the statistical and systematic contributions. Bottom panel: The ratios of the KNO scaled primary charged-particle distributions to the interpolated distribution at $\sqrt{s} = 13$ TeV are shown. Bands represent the uncertainties for the ratios as results of statistical and systematic uncertainties added in quadrature for both distributions

particles with $p_{\mathrm{T}} > 500$ MeV. These figures are similar to Figs. 2 and 3 but the vertical axis is stretched by the factor $\langle n_{\mathrm{ch}}(\sqrt{s}, p_{\mathrm{T}}^{\mathrm{min}})\rangle$.

The quantities of interest are derived from the original set of nine KNO distributions and the ratios of these distributions to the one at 13 TeV. The high-multiplicity tail of distributions is pushed up and the maximum of the distribution is shifted towards small values of z with collision energy increase.

Ratios of the KNO distributions between the smallest centre-of-mass energy 0.9 and 13 TeV exceed the maximum positive value at $z \approx 0.8$ and the maximum negative value for the highest multiplicity at $z \approx 5.5$ for $p_{\mathrm{T}} > 100$ MeV (Fig. 4a) and $z \approx 6.5$ for $p_{\mathrm{T}} > 500$ MeV (Fig. 5a). There is an intersection point for all distributions at $z \approx 2$.

A test of the KNO scaling distributions between $\sqrt{s} = 0.9$ and 13 TeV confirms that KNO scaling violation increases with decreasing collision energy. Ratios of the KNO distributions between the highest energies 8 and 13 TeV exceed the maximum value of $+8\%$ at $z \approx 0.5$ and the minimum value of -15% at $z \approx 0.1$ for $p_{\mathrm{T}} > 100$ MeV (Fig. 4b) and the maximum value of $+5\%$ at $z \approx 0.5$ and -13% at $z \approx 0.1$ for $p_{\mathrm{T}} > 500$ MeV (Fig. 5b). For the high multiplicity tail, these ratios are in agreement within error bars with the KNO distribution at 13 TeV.

Single- and double-diffractive processes give an important contribution only for the low multiplies region, $z \lesssim 0.3$. The typologies of diffractive and non-diffractive events are different and their KNO behavior may be also different. The negative spread, $\lesssim -8\%$, for the low multiplicity may be the results of diffractive processes contributing.

The KNO scaling tends to be independent of energy at $\sqrt{s} = 8$ and 13 TeV within $\approx {}^{+8}_{-15}\%$ for $z \lesssim 2$ and within error bars for $z \gtrsim 2$ for events with charged-particle transverse momentum $p_{\mathrm{T}} > 100$ MeV (Fig. 4b), and within ${}^{+5}_{-13}\%$ for $z \lesssim 3$ and within error bars for $z \gtrsim 3$ for events with charged-particle transverse momentum $p_{\mathrm{T}} > 500$ MeV (Fig. 5b). The tendency of the KNO scaling to hold for the highest collision energies is observed.

The MC QGSM predictions are made for the KNO non-diffractive charged-particle multiplicity distributions for pp collisions including at highest LHC centre-of-mass energy $\sqrt{s} = 14$ TeV for $|\eta| < 2.4$ on Fig. 12 in Ref. [43]. These distributions are the same qualitative behaviour as those presented in Fig. 4a. The MC QGSM described the KNO distributions as the contribution of the cylinder diagram and dia-

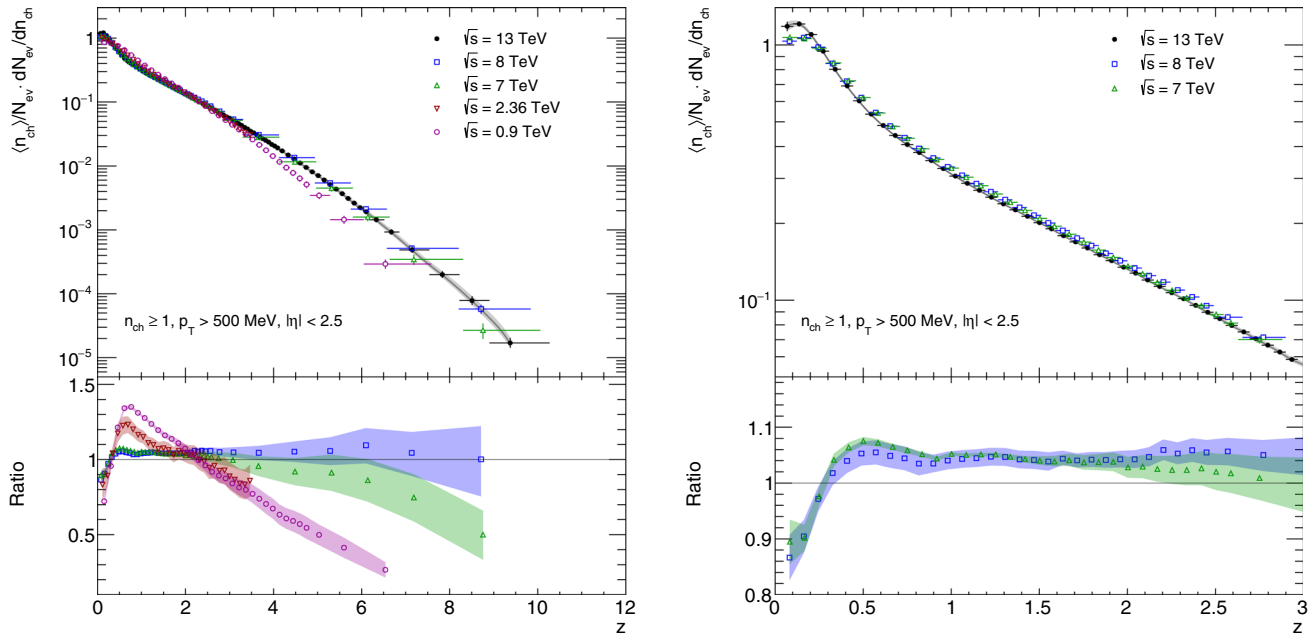

Fig. 5 Top panel: KNO scaled primary charged-particle multiplicity distributions as a function of the scaled multiplicity z, defined in Eq. (3), for events with $n_{\mathrm{ch}} \geq 1$, $p_{\mathrm{T}} > 500$ MeV and $|\eta| < 2.5$ measurement at the centre-of-mass energies 0.9, 2.36, 7, 8 and 13 TeV by the ATLAS [3–7] in **a** complete multiplicity region and **b** zoom multiplicity region with $z \leq 3$ at the $\sqrt{s} = 7$, 8 and 13 TeV. The gray curve and band of the uncertainties are the result of the interpolation of the charged-particle multiplicity distribution at 13 TeV. The uncertainties represent the sum in quadrature of the statistical and systematic contributions. Bottom panel: The ratios of the KNO scaled primary charged-particle distributions to the interpolated distribution at $\sqrt{s} = 13$ TeV are shown. Bands represent the uncertainties for the ratios as results of statistical and systematic uncertainties added in quadrature for both distributions

grams with multi-Pomeron scattering. The pronounced peak in the low z arises solely due to a single Pomeron exchange and the maxima of distributions for multi-Pomeron processes are moved in the direction of high z thus pushed up the tail [43].

4 Average transverse momentum dependences

The correct comparison of the primary charged-particle average transverse momentum, $\langle p_{\mathrm{T}} \rangle$, as a function of the scaled multiplicity z (3) for events with $n_{\mathrm{ch}} \geq 2$ and $p_{\mathrm{T}} > 100$ MeV; $n_{\mathrm{ch}} \geq 1$ and $p_{\mathrm{T}} > 500$ MeV for $|\eta| < 2.5$ measurement at the centre-of-mass energies from 0.9 to 13 TeV by the ATLAS [3–7] are presented in Fig. 6.

Figure 6a, b show an increase of the average transverse momentum distributions with the scaled multiplicity. The $\langle p_{\mathrm{T}} \rangle$ distribution as a function of z acquires higher value at higher collision energies. The value of $\langle p_{\mathrm{T}} \rangle$ increases by 18% and 13% for $z > 1$ with energy increase from 0.9 to 13 TeV for $p_{\mathrm{T}} > 100$ MeV and $p_{\mathrm{T}} > 500$ MeV, respectively. The results at 7 and 8 TeV are in agreement within error bars. The value of $\langle p_{\mathrm{T}} \rangle$ increases by $\approx 3\%$ for $p_{\mathrm{T}} > 100$ MeV and by $\approx 2.5\%$ for $p_{\mathrm{T}} > 500$ MeV with increase in energy from 8 to 13 TeV for $z > 0.5$. The ratio of $\langle p_{\mathrm{T}} \rangle$ for 8 to 13 TeV are in ≈ 6 times smaller than the ratio for 0.9 to 13 TeV.

5 Conclusion

The comparisons of the charged-particle multiplicity and the average transverse momentum distributions on the scaled multiplicity, KNO scale, using the results of the ATLAS collaboration at the LHC were presented. These distributions were measured in proton–proton collisions at centre-of-mass energies $\sqrt{s} = 0.9$, 2.36, 7, 8 and 13 TeV for the absolute pseudorapidity region less than 2.5 and for two events samples $n_{\mathrm{ch}} \geq 2$, $p_{\mathrm{T}} > 100$ MeV and $n_{\mathrm{ch}} \geq 1$, $p_{\mathrm{T}} > 500$ MeV. The charged-particle multiplicity distributions on the KNO scale have the similar shape and decrease with increasing energy. The study of the KNO scaling using the ATLAS results was done. A test of the KNO scaling between 0.9 and 13 TeV confirms that the KNO scaling violation increases with decreasing collision energy. The KNO distributions tend to be independent of energy for the highest energies. The

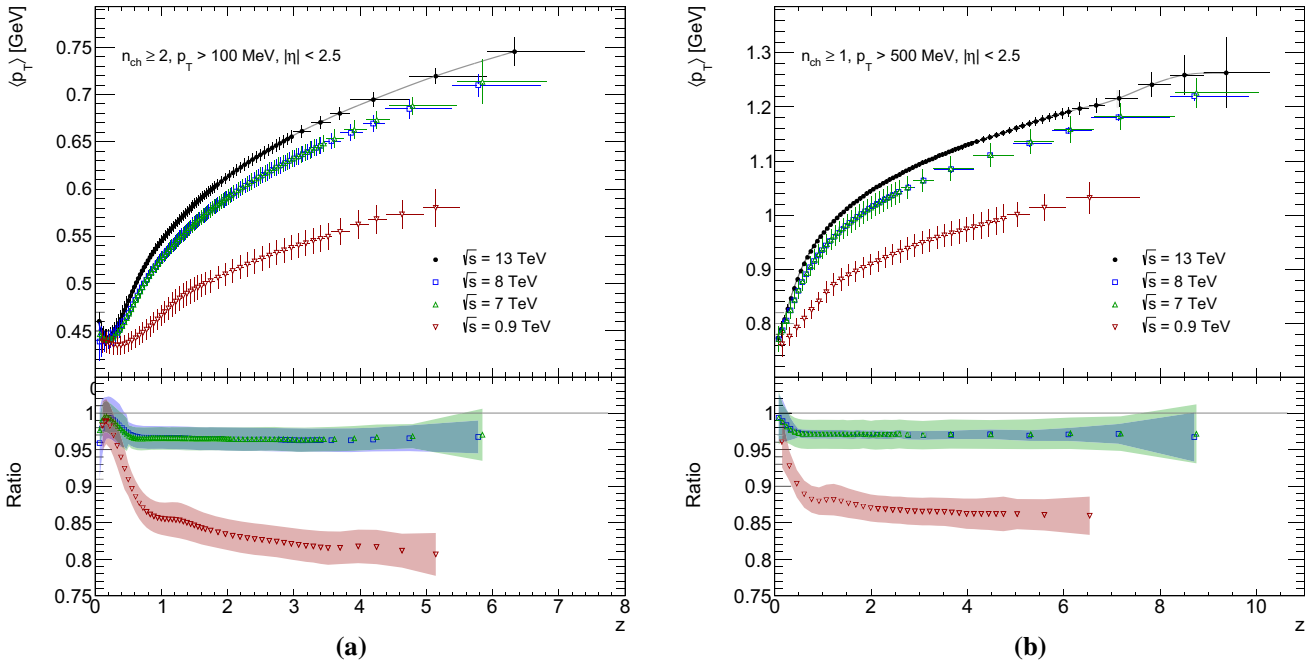

Fig. 6 Top panel: The average transverse momentum, $\langle p_T \rangle$, as a function of the scaled multiplicity z, defined in Eq. (3), for events with **a** $n_{ch} \geq 2$, $p_T > 100$ MeV and **b** $n_{ch} \geq 1$, $p_T > 500$ MeV for $|\eta| < 2.5$ measurement at the centre-of-mass energies 0.9, 7, 8 and 13 TeV by the ATLAS [3–7]. **a** The gray curve and band of the uncertainties are the result of the interpolation of the charged-particle multiplicity distribution at 13 TeV. The uncertainties are the result of the interpolation of the charged-particle multiplicity distribution at 13 TeV. The error bars and boxes represent the statistical and systematic contributions, respectively. Bottom panel: The ratios of the average transverse momentum distributions to the interpolated distribution at $\sqrt{s} = 13$ TeV are shown. Bands represent the uncertainties for the ratios as results of statistical and systematic uncertainties added in quadrature for both distributions

mean transverse momentum on the KNO scale has the same shape and increases with increasing energy.

Acknowledgements We thank the ATLAS collaboration for the excellent experimental results which were used for this analysis. Special thanks to E. K. Sarkisyan-Grinbaum and S. Ya. Tokar for several productive discussions. Thanks to E. E. Zabrodin for fruitful discussions concerning QGSM predictions. Useful discussions with V. V. Glagolev, G. I. Lykasov and N. A. Russakovich are gratefully acknowledged.

Data Availability Statement This manuscript has no associated data or the data will not be deposited. [Authors' comment: Data from all Figures and Table will be deposited in the Hepdata.]

Open Access This article is licensed under a Creative Commons Attribution 4.0 International License, which permits use, sharing, adaptation, distribution and reproduction in any medium or format, as long as you give appropriate credit to the original author(s) and the source, provide a link to the Creative Commons licence, and indicate if changes were made. The images or other third party material in this article are included in the article's Creative Commons licence, unless indicated otherwise in a credit line to the material. If material is not included in the article's Creative Commons licence and your intended use is not permitted by statutory regulation or exceeds the permitted use, you will need to obtain permission directly from the copyright holder. To view a copy of this licence, visit http://creativecommons.org/licenses/by/4.0/.
Funded by SCOAP[3].

References

1. L. Evans, P. Bryant, L.H.C. Machine, JINST **3**, S08001 (2008)
2. ATLAS Collaboration, The ATLAS Experiment at the CERN Large Hadron Collider, JINST **3**, S08003 (2008)
3. ATLAS Collaboration, Charged-particle multiplicities in pp interactions at $\sqrt{s} = 900$ GeV measured with the ATLAS detector at the LHC. Phys. Lett. B **688**, 21 (2010). arXiv:1003.3124 [hep-ex]
4. ATLAS Collaboration, Charged-particle multiplicities in pp interactions measured with the ATLAS detector at the LHC. New J. Phys. **13**, 053033 (2011). arXiv:1012.5104 [hep-ex]
5. ATLAS Collaboration, Charged-particle distributions in pp interactions at $\sqrt{s} = 8$ TeV measured with the ATLAS detector. Eur. Phys. J. C **76**, 403 (2016). arXiv:1603.02439 [hep-ex]
6. ATLAS Collaboration, Charged-particle distributions in $\sqrt{s} = 13$ TeV pp interactions measured with the ATLAS detector at the LHC. Phys. Lett. B **758**, 67 (2016). arXiv:1602.01633 [hep-ex]
7. ATLAS Collaboration, Charged-particle distributions at low transverse momentum in $\sqrt{s} = 13$ TeV pp interactions measured with the ATLAS detector at the LHC. Eur. Phys. J. C **76**, 502 (2016). arXiv:1606.01133 [hep-ex]
8. CMS Collaboration, The CMS Experiment at the CERN LHC. JINST **3**, S08004 (2008)
9. CMS Collaboration, Transverse momentum and pseudorapidity distributions of charged hadrons in pp collisions at $\sqrt{s} = 0.9$ and 2.36 TeV. JHEP **02**, 041 (2010). arXiv:1002.0621 [hep-ex]
10. CMS Collaboration, Transverse-momentum and pseudorapidity distributions of charged hadrons in pp collisions at $\sqrt{s} = 7$ TeV. Phys. Rev. Lett. **105**, 022002 (2010). arXiv:1005.3299 [hep-ex]

11. CMS Collaboration, Charged particle multiplicities in pp interactions at $\sqrt{s} = 0.9$, 2.36, and 7 TeV. JHEP **01**, 079 (2011). arXiv:1011.5531 [hep-ex]
12. CMS Collaboration, Pseudorapidity distribution of charged hadrons in proton–proton collisions at $\sqrt{s} = 13$ TeV. Phys. Lett. B **751**, 143 (2015). arXiv:1507.05915 [hep-ex]
13. CMS Collaboration, Measurement of charged particle spectra in minimum-bias events from proton–proton collisions at $\sqrt{s} = 13$ TeV. Eur. Phys. J. C **78**, 697 (2018). arXiv:1806.11245 [hep-ex]
14. TOTEM Collaboration, The TOTEM experiment at the CERN large hadron collider. JINST **3**, S08007 (2008)
15. CMS, TOTEM Collaborations, Measurement of pseudorapidity distributions of charged particles in proton–proton collisions at $\sqrt{s} = 8$ TeV by the CMS and TOTEM experiments. Eur. Phys. J. C **74**, 3053 (2014). arXiv:1405.0722 [hep-ex]
16. TOTEM Collaboration, Measurement of the forward charged particle pseudorapidity density in pp collisions at $\sqrt{s} = 8$ TeV using a displaced interaction point. Eur. Phys. J. C **75**, 126 (2015). arXiv:1411.4963 [hep-ex]
17. ALICE Collaboration, The ALICE experiment at the LHC. Phys. Part. Nucl. **39**, 1074 (2008)
18. ALICE Collaboration, Charged-particle multiplicity measurement in proton–proton collisions at $\sqrt{s} = 0.9$ and 2.36 TeV with ALICE at LHC. Eur. Phys. J. C **68**, 89 (2010). arXiv:1004.3034 [hep-ex]
19. ALICE Collaboration, Charged-particle multiplicity measurement in proton–proton collisions at $\sqrt{s} = 7$ TeV with ALICE at LHC. Eur. Phys. J. C **68**, 345 (2010). arXiv:1004.3514 [hep-ex]
20. ALICE Collaboration, Pseudorapidity and transverse-momentum distributions of charged particles in proton–proton collisions at $\sqrt{s} = 13$ TeV. Phys. Lett. B **753**, 319 (2016). arXiv:1509.08734 [nucl-ex]
21. ALICE Collaboration, Charged-particle multiplicities in proton–proton collisions at $\sqrt{s} = 0.9$ to 8 TeV. Eur. Phys. J. C **77**, 33 (2017). arXiv:1509.07541 [nucl-ex]
22. ALICE Collaboration, Charged-particle multiplicity distributions over a wide pseudorapidity range in proton–proton collisions at $\sqrt{s} = 0.9$, 7, and 8 TeV. Eur. Phys. J. C **77**, 852 (2017). arXiv:1708.01435 [hep-ex]
23. ALICE Collaboration, Charged-particle production as a function of multiplicity and transverse spherocity in pp collisions at $\sqrt{s} = 5.02$ and 13 TeV. Eur. Phys. J. C **79**, 857 (2019). arXiv:1905.07208 [nucl-ex]
24. LHCb Collaboration, The LHCb detector at the LHC. JINST **3**, S08005 (2008)
25. LHCb Collaboration, Measurement of charged particle multiplicities in pp collisions at $\sqrt{s} = 7$ TeV in the forward region. Eur. Phys. J. C **72**, 1947 (2012). arXiv:1112.4592 [hep-ex]
26. LHCb Collaboration, Measurement of charged particle multiplicities and densities in pp collisions at $\sqrt{s} = 7$ TeV in the forward region. Eur. Phys. J. C **74**, 2888 (2014). arXiv:1402.4430 [hep-ex]
27. CDF Collaboration, Pseudorapidity distributions of charged particles produced in $\bar{p}p$ interactions at $\sqrt{s} = 630$ GeV and 1800 GeV. FERMILAB-PUB-89-201-E, p. 119 (1989), ed. by J. Tran Thanh Van
28. CDF Collaboration, Measurement of particle production and inclusive differential cross sections in $p\bar{p}$ collisions at $\sqrt{s} = 1.96$-TeV. Phys. Rev. D **79**, 112005 (2009). arXiv:0904.1098 [hep-ex] [Erratum: Phys. Rev. D **82**, 119903 (2010)]
29. UA4 Collaboration, Pseudorapidity distribution of charged particles in diffraction dissociation events at the CERN SPS collider. Phys. Lett. B **166**, 459 (1986)
30. UA5 Collaboration, An investigation of multiplicity distributions in different pseudorapidity intervals in anti-p p reactions at a CMS energy of 540-GeV. Phys. Lett. B **160**, 193 (1985)
31. UA5 Collaboration, Charged particle multiplicity distributions at 200-GeV and 900-GeV center-of-mass energy. Z. Phys. C **43**, 357 (1989), ed. by R. Kotthaus and J. H. Kuhn
32. UA1 Collaboration, A study of the general characteristics of $p\bar{p}$ collisions at $\sqrt{s} = 0.2$-TeV to 0.9-TeV. Nucl. Phys. B **335**, 261 (1990)
33. A.M. Polyakov, A similarity hypothesis in the strong interactions. 1. Multiple hadron production in e^+e^- annihilation. Zh. Eksp. Teor. Fiz. **59**, 542 (1970)
34. Z. Koba, H.B. Nielsen, P. Olesen, Scaling of multiplicity distributions in high-energy hadron collisions. Nucl. Phys. B **40**, 317 (1972)
35. Z. Koba, Multi-body phenomena in strong interactions—description of hadronic multi-body final states, in *Proceedings CERN-JINR School of Physics, Ebeltoft, Denmark, 17–13 Jun 1973, CERN Yellow Reports: School Proceedings* (1973), p. 171
36. R.P. Feynman, Very high-energy collisions of hadrons. Phys. Rev. Lett. **23**, 1415 (1969), ed. by L.M. Brown
37. J.F. Grosse-Oetringhaus, K. Reygers, Charged-particle multiplicity in proton–proton collisions. J. Phys. G **37**, 083001 (2010). arXiv:0912.0023 [hep-ex]
38. S. Hegyi, KNO scaling 30 years later. Nucl. Phys. B Proc. Suppl. **92**, 122 (2001), ed. by A. Giovannini and R. Ugoccioni. arXiv:hep-ph/0011301
39. A.B. Kaidalov, The quark-gluon structure of the Pomeron and the rise of inclusive spectra at high-energies. Phys. Lett. B **116**, 459 (1982)
40. A.B. Kaidalov, K.A. Ter-Martirosian, Pomeron as quark-gluon strings and multiple hadron production at SPS collider energies. Phys. Lett. B **117**, 247 (1982)
41. V.N. Gribov, A Reggeon diagram technique. Zh. Eksp. Teor. Fiz. **53**, 654 (1967)
42. V.N. Gribov, E.M. Levin, M.G. Ryskin, Semihard processes in QCD. Phys. Rep. **100**, 1 (1983)
43. J. Bleibel, L.V. Bravina, A.B. Kaidalov, E.E. Zabrodin, How many of the scaling trends in pp collisions will be violated at $\sqrt{s_{NN}} = 14$ TeV?—Predictions from Monte Carlo quark-gluon string model. Phys. Rev. D **93**, 114012 (2016). arXiv:1011.2703 [hep-ph]
44. L.V. Bravina, E.E. Zabrodin, Scaling trends in proton–proton collisions from SPS to LHC in quark-gluon string model. J. Phys. Conf. Ser. **668**, 012045 (2016), ed. by D. Alvarez-Castillo, D. Blaschke, V. Kekelidze, V. Matveev and A. Sorin
45. W. Kittel, E.A. De Wolf, Soft multihadron dynamics. World Scientific Singapore; Hackensack, NJ, (2005). ISBN:978-981-256-295-1
46. I.M. Dremin, J.W. Gary, Hadron multiplicities. Phys. Rep. **349**, 301 (2001). arXiv:hep-ph/0004215
47. ATLAS Collaboration, Two-particle Bose–Einstein correlations in pp collisions at $\sqrt{s} = 13$ TeV measured with the ATLAS detector at the LHC. Submitted to Eur. Phys. J. C (2022). arXiv:2202.02218 [hep-ex]
48. I. Antcheva et al., ROOT: a C++ framework for petabyte data storage, statistical analysis and visualization. Comput. Phys. Commun. **180**, 2499 (2009). arXiv:1508.07749 [physics.data-an]